Journal of Solid State Chemistry 184 (2011) 2566–2570

Contents lists available at ScienceDirect

Journal of Solid State Chemistry

journal homepage: www.elsevier.com/locate/jssc

Host-sensitized emission of $LiInW_2O_8$ wolframites: From red-Eu^{3+} to white-Dy^{3+} phosphors

S. Asiri Naidu [a], S. Boudin [a,*], U.V. Varadaraju [b], B. Raveau [a]

[a] Laboratoire CRISMAT (CNRS UMR6508), ENSICAEN, Université de Caen, 6 Bd. Maréchal Juin, 14050 Caen Cedex, France
[b] Department of Chemistry, Indian Institute of Technology Madras, Chennai 600036, India

ARTICLE INFO

Article history:
Received 10 June 2011
Received in revised form
15 July 2011
Accepted 16 July 2011
Available online 22 July 2011

Keywords:
$LiInW_2O_8$ wolframite
Host sensitization
Photoluminescence
Energy transfer

ABSTRACT

The $LiInW_2O_8$:Eu^{3+}, $LiInW_2O_8$:Dy^{3+} and $LiInW_2O_8$:Eu^{3+}/Dy^{3+} phosphors were synthesized by solid-state reaction and their photoluminescence properties were studied. Under UV excitation, the $LiInW_2O_8$:Eu^{3+} phosphor exhibits an intense red emission whereas the $LiInW_2O_8$:Dy^{3+} and $LiInW_2O_8$:Dy^{3+}/Eu^{3+} phosphors show a white emission. The WO_6 octahedra play a major role in the luminescence of the host lattice, characterized by a blue emission under UV excitation. The emission of activator ion results from an efficient energy transfer from the $LiInW_2O_8$ host lattice to the Eu^{3+} and Dy^{3+} ions. The $LiIn_{0.97}Dy^{3+}_{0.03}W_2O_8$ and $LiIn_{0.965}$ $Dy^{3+}_{0.03}Eu^{3+}_{0.005}W_2O_8$ samples, optimized for white emission, are interesting candidates for solid-state lighting applications.

1. Introduction

Double tungstates activated with rare-earth ions have drawn a considerable interest in the field of solid-state lighting, solid-state lasers and inorganic scintillation applications. The main reason for this is due to their efficient radiative emissions in the visible and mid-infrared spectral regions. The Ln^{3+} lanthanide ions (except Ce^{3+}), which are stable under ambient conditions, exhibit a narrow bands emission, due to *f–f* transitions. Ln^{3+} ions have been playing a vital role in the solid-state lighting and display fields due to their abundant emission colors, based on their 4*f*–4*f* or 5*d*–4*f* transitions [1]. The *f–f* transitions Ln^{3+} ions have low excitation efficiencies because of their forbidden parity selection rules. So, the energy transfer from some foreign species to Ln^{3+} ions seems very crucial in enhancing the luminescence efficiency of Ln^{3+} ions. Host sensitization of Ln^{3+} ions is the important route to retrieve the efficient emission of Ln^{3+} ions as shown, for example for YVO_4:Eu^{3+}, $CaIn_2O_4$:Dy^{3+} and $SrIn_2O_4$:Dy^{3+} [2–4]. Trivalent dysprosium (Dy^{3+}) exhibits various potential applications as an activator, in plasma display panels, field emission displays and mercury free lamps [5–9]. Dy^{3+} emission mainly consists of a blue (470–500 nm, $^4F_{9/2}$–$^6H_{15/2}$) and a yellow (570–600 nm, $^4F_{9/2}$–$^6H_{13/2}$) narrow bands [10]; as a result Dy^{3+} emits white light in most of the host lattices at a suitable yellow-to-blue intensity ratio. Trivalent europium (Eu^{3+}) ion is a well-known red emitting activator due to its $^5D_0$–^7F_J (J=0, 1, 2, 3, 4) transitions [1]. Interestingly, the $LiInW_2O_8$:Tm^{3+} double tungstate with the wolframite structure was recently reported to be a promising blue phosphor [11] for field emission displays. Curiously, the luminescent properties of this wolframite series have not been explored further for other activators. In particular the possibility of getting white light from single activator ion in this series has not been studied. The problem with the multiple activator ions is to find a suitable excitation wavelength in order to produce white light generation. With this view, in the present study, we have studied the photoluminescence (PL) properties of Eu^{3+} and Dy^{3+} doped tungstates $LiIn_{1-x}Eu_xW_2O_8$ and $LiIn_{1-x}Dy_xW_2O_8$. Previously, in order to understand the role played by the tungstates host, we have studied the undoped phases $LiInW_2O_8$ and $LiScW_2O_8$ using X-ray diffraction, diffuse reflectance and photoluminescence (PL).

2. Experimental

Phases $LiIn_{1-x}Eu_xW_2O_8$ (x=0.0, 0.03, 0.05, 0.07, 0.1), $LiIn_{1-x}Dy_xW_2O_8$ (x=0.01, 0.03, 0.05, 0.07, 0.1), $LiIn_{0.965}Dy_{0.03}Eu_{0.005}W_2O_8$ and $LiScW_2O_8$ were prepared by the solid-state reaction as reported in the literature [11,12]. The starting materials used were Li_2CO_3 (99%, Aldrich), In_2O_3 (99.9%, Alfa Aesar), Sc_2O_3 (99.99%, Alfa Aesar), WO_3 (99.8%, Alfa Aesar), Dy_2O_3 and Eu_2O_3 (99.9%, Alfa Aesar). Dy_2O_3 and Eu_2O_3 were preheated at 900 °C overnight. The stoichiometric precursors were intimately ground, placed in a platinum crucible and

* Corresponding author. Fax: 33 2 31 95 16 00.
E-mail address: sophie.boudin@ensicaen.fr (S. Boudin).

0022-4596/$ - see front matter © 2011 Elsevier Inc. All rights reserved.
doi:10.1016/j.jssc.2011.07.029

fired at 700 °C for 15 h and 950 °C for 15 h. The synthesis conditions for $LiScW_2O_8$ were 1000 °C for 48 h with intermediate grindings.

Powder X-ray diffraction data were recorded for all the above samples, using a Panalytical X'pert Pro X-ray diffractometer with a Cu $K\alpha$ source ($\lambda = 1.5418$ Å). No impurity phases were detected. Crystal structure of the parent $LiInW_2O_8$ phase was refinement by the Rietveld method using the Fullprof program [13]. Complete details of the refinement can be downloaded in CIF format as supplementary materials.

Diffuse reflectance spectra were measured by using a CARY 100 Varian spectrophotometer over the spectral range of 200–800 nm (with 1 nm steps). $BaSO_4$ was used as a reference for 100% reflectance. Excitation and emission spectra were recorded (with 1 nm steps) by using a Fluorolog-3 Horiba Jobin Yvon spectrofluorometer equipped with a 450 W Xenon lamp. All measurements have been carried out at room temperature.

3. Results and discussion

3.1. Structural analysis of $LiInW_2O_8$

$LiInW_2O_8$, isotypic to the $LiFeW_2O_8$ wolframite, crystallizes in the $C2/c$ monoclinic symmetry [14]. In the crystal structure, the WO_6 octahedra share edges forming $[WO_4]_\infty$ zigzag chains along the c-direction (Fig. 1). The InO_6 octahedra, linked by corner to the WO_6 octahedra, ensure the connection between the $[WO_4]_\infty$ chains. The Li^+ ions, in octahedral coordination, are located in tunnels running along c and bordered by $[WO_4]_\infty$ chains and InO_6 octahedra. The refined lattice parameters and the agreement factors are given in Table 1. The atomic parameters and distances of $LiInW_2O_8$ are given in Tables 2 and 3, respectively. The observed, calculated and difference diffractograms of $LiInW_2O_8$ are shown in Fig. 2. Compared to $LiFeW_2O_8$, $LiInW_2O_8$ phase exhibit larger cell parameters and cell volume in agreement with the larger size of In^{3+} radius ($r(In^{3+}) = 0.94$ Å $> r(Fe^{3+}) = 0.785$ Å [15]). In both structures, the WO_6 and LiO_6 octahedra exhibit comparable expansion with close average W–O distances (equal to 1.94(1) Å in $LiInW_2O_8$ against 2.01(8) Å in $LiFeW_2O_8$) and Li–O distances (equal to 2.20(1)Å in $LiInW_2O_8$ against 2.12(8)Å in $LiFeW_2O_8$). The MO_6 octahedron (M=In, Fe) is logically more expanded in $LiInW_2O_8$ structure in agreement with the larger size of In^{3+} radius (with average In–O distances equal to 2.14(1) Å and average Fe–O distances equal to 1.93(8) Å).

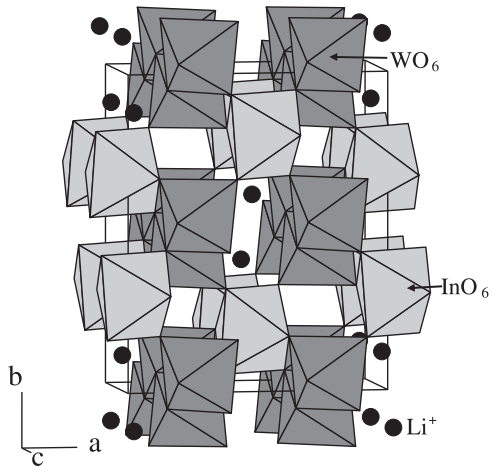

Fig. 1. Projection of $LiInW_2O_8$ structure (WO_6 and InO_6 octahedra are represented in dark and light gray, respectively, Li^+ ions with black balls).

Table 1
Cell parameters and agreement factors for $LiInW_2O_8$.

$LiInW_2O_8$	
Space group	$C2/c$ (no15)
a (Å)	9.58096(1)
b (Å)	11.59048(2)
c (Å)	4.95688(1)
β (deg.)	91.0820(1)
Cell volume (Å^3)	550.353(2)
R_{Bragg} (%)	8.37
R_f (%)	5.33
R_p (%)	5.04
R_{wp} (%)	6.75
R_{exp} (%)	1.55

Table 2
Atomic parameters for $LiInW_2O_8$.

Atom	Wyckoff position	X	y	z	B_{iso} (Å^2)	Site occupation (%)
W	8f	0.2424(1)	0.08932(8)	0.2506(3)	0.21(2)	100
In	4e	0.	0.3389(3)	0.25	0.53(4)	100
Li	4e	0.5	0.3412(6)	0.25	1.0[a]	100
O(1)	8f	0.358(1)	0.050(1)	0.938(3)	0.8(1)	100
O(2)	8f	0.388(1)	0.169(1)	0.387(2)	0.8(1)	100
O(3)	8f	0.352(1)	0.549(1)	0.943(3)	0.8(1)	100
O(4)	8f	0.381(1)	0.688(1)	0.404(2)	0.8(1)	100

[a] fixed parameters.

Table 3
Distances (Å) in $LiInW_2O_8$.

W–O(1)	1.98(1)	In–O(1)	2.10(1) × 2
W–O(1)	2.16(1)	In–O(2)	2.08(1) × 2
W–O(2)	1.79(1)	In–O(4)	2.23(1) × 2
W–O(3)	1.84(1)	$\overline{In-O}$	2.14(1)
W–O(3)	2.07(1)		
W–O(4)	1.81(1)	Li–O(2)	2.37(2) × 2
$\overline{W-O}$	1.94(1)	Li–O(3)	2.15(1) × 2
		Li–O(4)	2.07(1) × 2
		$\overline{Li-O}$	2.20(1)

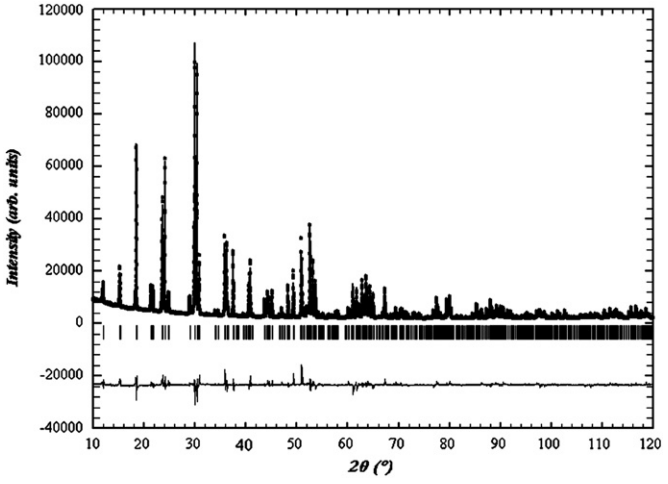

Fig. 2. X-ray powder diffraction patterns of $LiInW_2O_8$ (observed, calculated and difference patterns are represented with dots, bold line and solid line, respectively; positions of Bragg reflections with vertical bars).

3.2. Diffuse reflectance spectroscopy

The diffuse reflectance spectra of $LiInW_2O_8$ and $LiScW_2O_8$ tungstates are shown in Fig. 3. The deduced band gap values calculated from the Kubelka–Munk function are ~3.85 and ~3.89 eV, respectively, for $LiInW_2O_8$ and $LiScW_2O_8$, in good agreement with the more covalent character of In–O bonds compared to Sc–O bonds. For both tungstates, the maximum absorption peaks are observed at around 295 nm.

3.3. Photoluminescence (PL) properties

PL excitation and emission spectra of $LiInW_2O_8$ are presented in Fig. 4. Under UV excitation at 297 nm, $LiInW_2O_8$ exhibits a blue emission centered at 458 nm as found by Derbal et al. [11]. The blue emission can originate from the transitions within the indium or tungsten octahedral host lattice. Indeed, blue luminescence under UV irradiation has previously been observed either in pure tungstate matrices such as $KLuW_2O_8$ and $AgLaW_2O_8$ [16,17] or in pure indate matrices such as $LaInO_3$, $CaIn_2O_4$ or $SrIn_2O_4$ [3–4,18]. In order to understand the role of each type of octahedra in the luminescence, we have studied the isotypic $LiScW_2O_8$ tungstate. We observe that the latter exhibits, like $LiInW_2O_8$, a weak blue emission (458 nm) under a 295 nm excitation (Fig. 4). Thus, we can clearly conclude that the WO_6 octahedra play a major role in the blue emission of both, $LiInW_2O_8$ and $LiScW_2O_8$. The intrinsic luminescence of tungstate compound is due to the $^3T_1$ and $^3T_2 \rightarrow {}^1A_1$ spin-forbidden electronic transitions [19].

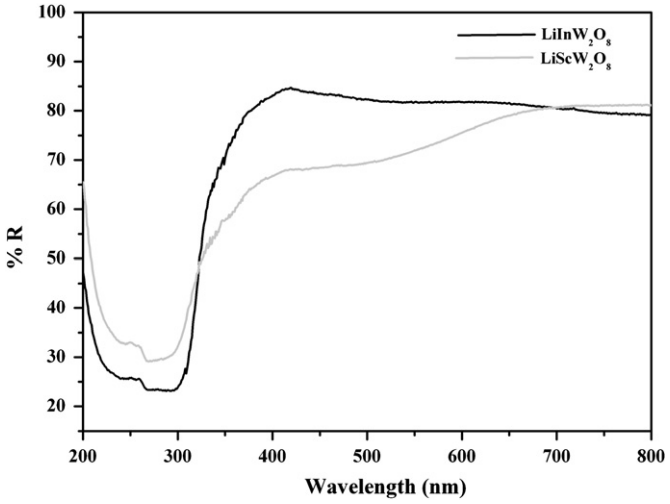

Fig. 3. Diffuse reflectance spectra of $LiInW_2O_8$ and $LiScW_2O_8$.

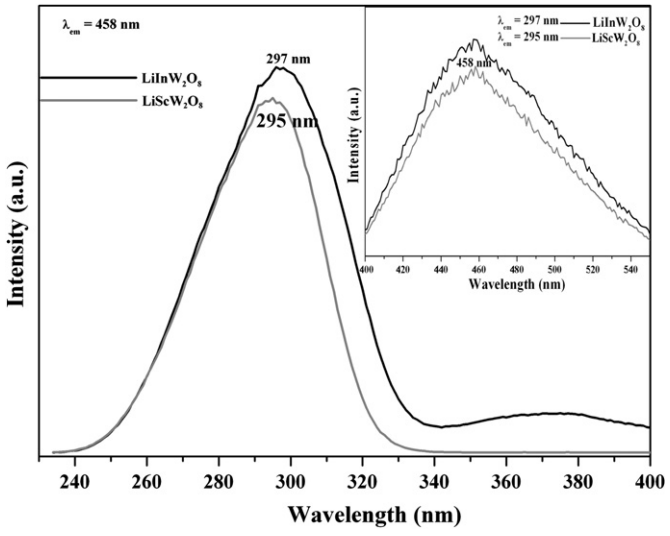

Fig. 4. Excitation spectra of $LiInW_2O_8$ and $LiScW_2O_8$ (inset shows the emission spectra of $LiInW_2O_8$ and $LiScW_2O_8$).

Fig. 5a shows the excitation spectrum of $LiIn_{0.95}Eu_{0.05}W_2O_8$ recorded with 612 nm emission. The excitation spectrum consists of a strong excitation band around 200–350 nm with a maximum at 297 nm, which is attributed to the host lattice absorption (Fig. 4). The Eu^{3+}–O^{2-} charge transfer band (CTB) is not conspicuous in the excitation spectrum, probably due to the overlap with the host absorption band. The peaks at 395 ($^7F_0$–$^5L_6$) and 465 nm ($^7F_0$–$^5D_2$) are due to the intra-*f*–*f* electronic transitions of the Eu^{3+} ion. The emission spectrum of this phase under 297 nm (host absorption) is shown in Fig. 5b. The emission spectrum consists of groups of lines between 575 and 725 nm corresponding to $^5D_0$–^7F_J (J=0–4) transitions of Eu^{3+} [20]. The $^5D_0$–$^7F_2$ electric dipole transition at 612 nm is dominant, which confirmed that the In^{3+} site occupied by Eu^{3+} has no inversion center in agreement with the crystal structure. No broad emission at 458 nm corresponding to the host lattice is observed in $LiIn_{0.95}Eu_{0.05}W_2O_8$ compound. This indicates an efficient energy transfer from the host to the Eu^{3+} ion.

The change in the emission intensity with Eu^{3+} content is followed by monitoring of the intensity of the 612 nm peak ($^5D_0$–$^7F_2$) under 297 nm excitation (Fig. 6). The emission intensity increases with increasing the Eu^{3+} content from 0.03 to 0.1 in $LiIn_{1-x}Eu_xW_2O_8$; beyond x=0.1, PL was not studied because unidentified impurities were detected by the X-ray diffraction. The concentration quenching of $LiIn_{1-x}Eu_xW_2O_8$ (not observed but probably at $x \geq 0.1$) differs from that of $LiIn_{1-x}Tm_xW_2O_8$ equal to x=0.05 [11].

The excitation spectrum of $LiIn_{0.97}Dy_{0.03}W_2O_8$ monitored with 580 nm (Fig. 7a) consists of a strong excitation band between 200 and 350 nm with a maximum at 299 nm, due to the host absorption. The weak transitions in the longer wavelength region are due to the $4f^9$–$4f^9$ transitions of the Dy^{3+} cations [1]. In the case of Eu^{3+} the charge transfer absorption band is located in the UV region. This is not the case for Dy^{3+}, the charge transfer band and $4f^9$–$4f^8 5d$ bands of Dy^{3+} are located below 200 nm [10] and direct UV excitation of Dy^{3+} through forbidden *f*–*f* transitions is weak. This drawback of Dy^{3+} excitation can be overcome by either host or ion sensitization. The emission spectrum of Dy^{3+} in

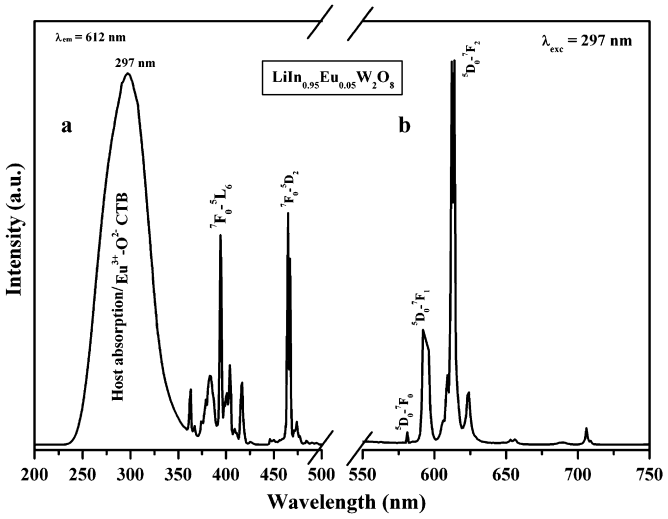

Fig. 5. Excitation and emission spectra of $LiIn_{0.95}Eu_{0.05}W_2O_8$.

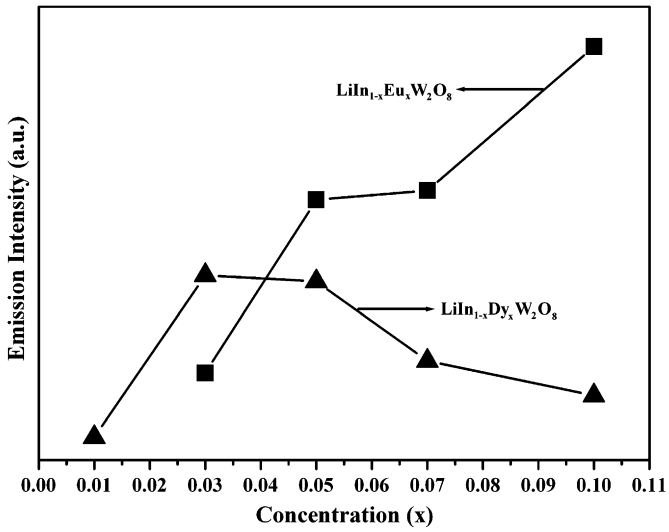

Fig. 6. Concentration dependence of Eu^{3+} ($^5D_0$–$^7F_2$) and Dy^{3+} ($^4F_{9/2}$–$^6H_{13/2}$) emission intensities in $LiIn_{1-x}Eu_xW_2O_8$ and $LiIn_{1-x}Dy_xW_2O_8$ respectively.

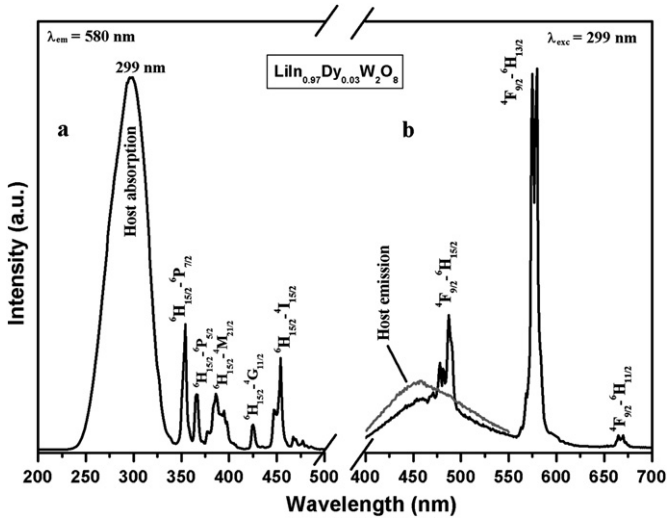

Fig. 7. Excitation and emission spectra of $LiIn_{0.97}Dy_{0.03}W_2O_8$.

$LiIn_{0.97}Dy_{0.03}W_2O_8$ under host excitation (299 nm) shows emission transitions at 487 nm ($^4F_{9/2}$–$^6H_{15/2}$, blue), 580 nm ($^4F_{9/2}$–$^6H_{13/2}$, yellow) (Fig. 7b). It is known that the blue $^4F_{9/2}$–$^6H_{15/2}$ transition at 487 nm originates from magnetic dipole and the yellow one $^4F_{9/2}$–$^6H_{13/2}$ at 580 nm originates from electric dipole. $^4F_{9/2}$–$^6H_{13/2}$ is dominant only when the Dy^{3+} ions occupy sites, with no inversion centers [21]. The dominant 580 nm emission is in agreement with the crystal structure where Dy^{3+} lies on the In^{3+} site located on a twofold axis. The host blue emission band in $LiIn_{0.97}Dy_{0.03}W_2O_8$ has an identical profile with that of the parent emission (represented with a gray line in Fig. 7b). The white color observed in the present work is the result of the mixture of weak blue (host emission, 400–470 nm), and Dy^{3+} main emissions (at 487 and 580 nm). The blue emission at 487 nm and the yellow one at 580 nm correspond to the $^4F_{9/2}$–$^6H_{15/2}$ and $^4F_{9/2}$–$^6H_{13/2}$ transitions, respectively, of the Dy^{3+} ions as observed for the phosphor $Na_2Sr(PO_4)F:Dy^{3+}$ [21]. These three emission bands combine to generate a spectrum in the visible region that appears white to the naked eye.

Variation in the concentration of activator ions can influence the emission of a phosphor. Generally, a low concentration of activator ion gives weak emission, but high concentrations of activator ion can cause quenching of emission. In the present study, the critical concentration of Dy^{3+} is found to be $x=0.03$ in $LiIn_{1-x}Dy_xW_2O_8$, beyond which concentration quenching occurs (Fig. 6). Usually the concentration quenching of the emission is due to transfer of energy among the activator ions at high activator concentrations. During the process the excitation energy will be lost to the killer sites non-radiatively and leads to a decrease of the PL emission intensity [1]. The concentration quenching of the Dy^{3+} emission is mainly due to the cross relaxation between neighboring Dy^{3+} ions which are in resonance of their energy levels due to the Dy^{3+}($^4F_{9/2}$)+Dy^{3+} ($^6H_{15/2}$)→ Dy^{3+}($^6F_{3/2}$)+ Dy^{3+} ($^6F_{11/2}$) transitions [19].

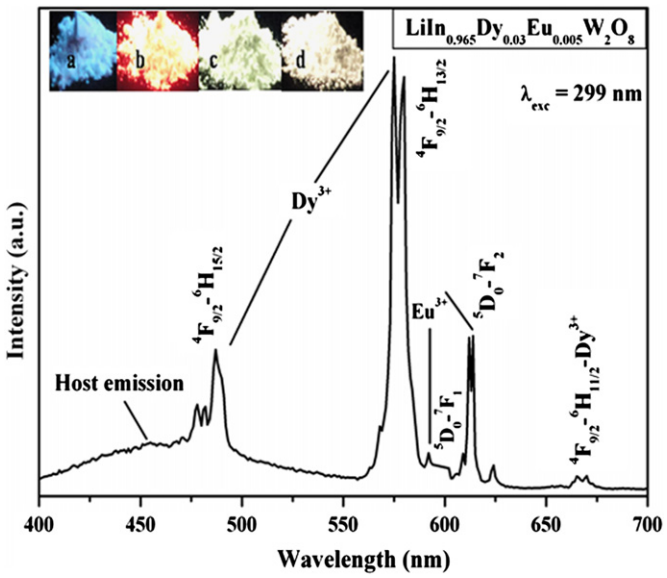

Fig. 8. Emission spectrum of $LiIn_{0.965}Dy_{0.03}Eu_{0.005}W_2O_8$. Inset shows images of (a) undoped; (b) 0.1 Eu^{3+} doped; (c) 0.03 Dy^{3+} doped and (d) 0.03 Eu^{3+}, 0.005 Dy^{3+} co-doped $LiInW_2O_8$ under a 254 nm external lamp.

In order to have a full-color-emitting phosphor that emits in the whole visible region (blue, green and red), which is required for solid-state lighting application, we have co-doped Eu^{3+} in $LiIn_{0.97}Dy_{0.03}W_2O_8$. The most notable feature from the excitation spectra (Figs. 5 and 7) is that by using selective excitation wavelengths (host excitation); it is possible to excite all the activators in order to obtain emission from Dy^{3+} and Eu^{3+}. An optimized red emission was found for $x=0.005$ Eu^{3+} content. The PL emission spectrum of Dy^{3+} co-doped with Eu^{3+} in $LiIn_{0.965}Dy_{0.03}Eu_{0.005}W_2O_8$ is shown in Fig. 8. The emission spectrum, with bands due to host lattice, Dy^{3+} and Eu^{3+}, covers the entire visible region from 400 to700 nm.

4. Conclusions

The $LiInW_2O_8:Eu^{3+}$, $LiInW_2O_8:Dy^{3+}$ and $LiIn_{0.965}Dy_{0.03}Eu_{0.005}W_2O_8$ phosphors were synthesized by the solid-state reaction. We have shown that the WO_6 octahedra play a major role in the host lattice luminescence and that there exists an energy transfer from $LiInW_2O_8$ host matrix to the activator ions (Eu^{3+}, Dy^{3+}). The PL results reveal the presence of Eu^{3+} and Dy^{3+} ions at non-centrosymmetric sites. The Dy^{3+} phosphors exhibits a critical concentration $x=0.03$ close to that of the Tm^{3+} phosphor ($x=0.05$). This behavior is different from that of the Eu^{3+} phosphor, whose emission intensity increases continuously up to $x=0.1$. Importantly, these three phosphors exhibit different emission under the host excitation, i.e., intense red for $LiInW_2O_8:Eu^{3+}$, and white for $LiInW_2O_8:Dy^{3+}$

and $LiIn_{0.965}Dy_{0.03}Eu_{0.005}W_2O_8$. Therefore, these phosphors may be considered as suitable candidates for solid-state lighting applications.

Supplementary materials

Crystal structure refinement details of $LiInW_2O_8$ can be downloaded as supplementary materials on a CIF format. Crystal structure of $LiInW_2O_8$ has been recorded on the Fachinformationszentrum Karlsruhe data base under the CSD-423127 reference.

Appendix A. Supplementary information

Supplementary data associated with this article can be found in the online version at doi:10.1016/j.jssc.2011.07.029.

References

[1] G. Blasse, B.C. Grabmaier, Luminescent Materials, Springer-Verlag, Berlin, Germany, 1994.
[2] M. Yu, J. Lin, Z. Wang, J. Fu, S. Wang, H.J. Zhang, Y.C. Han, Chem. Mater. 14 (2002) 2224–2231.
[3] X. Liu, R. Pang, Q. Li, J. Lin., J. Solid State Chem. 180 (2007) 1421–1430.
[4] X. Liu, C. Lin, Y. Luo, J. Lin., J. Electrochem. Soc. 154 (1) (2007) J21–J27.
[5] B. Han, K.C. Mishra, M. Raukas, K. Klinedinst, J. Tao, J.B. Talbot, J. Electrochem. Soc. 154 (2007) J44–J52.
[6] Y. Gong, Y.H. Wang, Y.Q. Li, X.H. Xu, J. Electrochem. Soc. 157 (2010) J208–J211.
[7] H. He, R.L. Fu, X.F. Song, R. Li, Z.W. Pan, X.R. Zhao, Z.H. Deng, Y.G. Cao, J. Electrochem. Soc. 157 (2010) J69–J73.
[8] J.P. Zhong, H.B. Liang, B. Han, Z.F. Tian, Q. Su, Opt. Express 16 (2008) 7508.
[9] K.M. Krishna, G. Anoop, M.K. Jayaraj, J. Electrochem. Soc. 154 (2007) J310–J313.
[10] E. Loh, Phys. Rev. 147 (1966) 332–335.
[11] M. Derbal, L. Guerbous, O. Djamel, C.J. Pierre, M. Kadi-Hanifi., Adv. Condens. Matter Phys. 2009 (2009) 327605–327612.
[12] P.N. Namboodiri, A.B. Phadnis, V.V. Deshpande., Thermochim. Acta 144 (1989) 151–157.
[13] Fullprof Suite Program (1.00) – version February 2007, Carvajal J.R. (ILL, France), Roisnel T. (LCSIM, CNRS, France), Platas J.G. (ULL, Spain), Chapon L.C. (ISIS, RAL, UK).
[14] P.V. Klevtsov, R.F. Klevtsova, Sov. Phys. Crystallogr. 15 (2) (1970) 245–248.
[15] R.D. Shannon, C.T. Prewitt, Acta Crystallogr. Sect. B Struct. Crystallogr. Cryst. Chem. 25 (1969) 925.
[16] G. Benoît, J. Véronique, A. Arnaud, G. Alain, Solid State Sci. 13 (2) (2011) 460–467.
[17] V. Sivakumar, U.V. Varadaraju, J. Electrochem. Soc. 153 (3) (2006) H54–H57.
[18] N. Lakshminarasimhan, U.V. Varadaraju, Mater. Res. Bull. 41 (2006) 724–731.
[19] G. Blasse, Struct. Bonding (Berlin) 42 (1980) 1.
[20] J. Hölsä, M. Leskelä, J. Lumin. 48/49 (1991) 497–500.
[21] I.M. Nagpure, V.B. Pawade, S.J. Dhoble, Luminescence 25 (2010) 9–13.